A Technique to Control the Harmonic Levels in Time Modulated Antenna Arrays – Theoretical Concept and Hardware Verification Platform

Edward A. Ball, *Member, IEEE* and Alan Tennant, *Member, IEEE*

***Abstract*—This paper presents techniques into prediction and control of the radiated harmonic levels in time modulated antenna arrays (TMAs). The effect of ramping on the controlling switching waveform, due to slew in the RF switches, is analyzed first. This is followed by a novel technique for controlling and reducing the fundamental carrier component (due to the Fourier series 0 Hz term) that is always produced by TMAs. A new bespoke, steerable, TMA RF hardware test platform is presented, using three gain states to pragmatically implement the proposed carrier reduction technique. The platform implementation utilizes binary logic control interfaces to the TMA, rather than analogue control interfaces. Laboratory measurements using the test platform demonstrate a 16.5dB reduction (limited by PCB emissions) in the level of the fundamental carrier component relative to the steered first harmonic, from a possible reduction of 21.3dB. The array gain for the first harmonic beam is 2dBi.**

***Index Terms*—Time Modulated Antenna Arrays, Fourier series, RF hardware platform, Microwave circuits.**

I. Introduction

THERE IS TODAY much ongoing research into beamforming techniques for use in next generation 5G communications, including a focus on mmWave radio for mobile applications [1]. From a future mobile device's perspective, it can be argued that only a single active beam may be required at any particular instant; significantly relaxing the technical challenge and cost in implementing a radio using beamforming.

The time modulated antenna array (TMA) [2], [3], [4], [5], [6] can be used to generate a beam at a desired angle without the use of vector modulators or phase shifters, though it seems rarely used in practice. TMAs create a steerable beam, using only RF switching elements and can create or receive multiple beams carrying different modulated data [7], [8] or steer nulls in the direction of interference [9], [10], [11], [12]. The TMA has also been investigated for use in direction finding systems [13], [14] by analyzing signal harmonic characteristics. TMAs are also applicable to radar systems [15], [16] and can incorporate both a radar function in the boresight beam and a communications function in the other beams, using a single system [17], [18], [19]. The TMA has also seen application in reflector arrays [20], for diversity reception systems [21], and multiple beam communications [22]. Recently TMAs have found use in generating orbital angular momentum waves [23], [24] and circular polarization [25]. Most systems use only the boresight beam or possibly the first harmonic beam, with increased beam steer angles requiring the use of higher order harmonics for realizable switching timings.

In this paper we devise concepts to predict and control the level of the harmonic beams including, for the first time to our knowledge, a new technique to control or cancel the fundamental beam at boresight. In section II of this paper we briefly introduce the concept of TMAs and then go on to predict the magnitude of a harmonic beam as a function of RF switch ramping time between on and off states, due to slew rate. We then propose a new way of controlling the harmonic fundamental beam magnitude due to the Fourier series 0 Hz term, using a bipolar gain stage. Section III introduces a 5.8GHz RF hardware switching architecture, using three gain states and phase inversions per array element to implement the required bipolar gain, leading to a novel RF TMA test platform. In section IV we present measured data from radiated chamber tests of the six element TMA array. We conclude the paper in section V.

The contributions of this paper are threefold: 1) mathematical model for the prediction of harmonic levels in TMAs due to RF switching slew; 2) Novel algorithm and RF hardware technique to null out the TMA fundamental component at the carrier frequency without affecting the harmonic beam steering; and 3) proof of concept test results from laboratory tests using the bespoke RF hardware platform.

II. Harmonic Levels In Time Modulated Arrays

TMAs use switching time to control the direction of a harmonic beam carrying RF energy. Often in TMA design, the fundamental component at the carrier is the focus of attention and all other harmonics are to be curtailed. There has been some research into controlling the magnitude of these harmonic levels, for example using trapezoid switching

Manuscripted submitted 10th of April 2019; revised 10th January 2020.

E. A. Ball is with the Department of Electronic and Electrical Engineering at the University of Sheffield, Sheffield, United Kingdom (e-mail: e.a.ball@sheffield.ac.uk).

A. Tennant is with the Department of Electronic and Electrical Engineering at the University of Sheffield, Sheffield, United Kingdom (e-mail: a.tennant@sheffield.ac.uk).

waveforms and cosine switching waveforms [26], [27], though these can require complex circuitry to implement the required analogue control waveforms. There has also been investigation into the control of the instantaneous emission level [28], which can be significant in TMAs. In this paper we only consider the average emission level, as would be perceived by a receiver of the beam from a linear array.

A. TMA with RF Switching Slew

The Array Factor (AF) for an array of *N* isotropic radiating elements in a TMA can be described by (1) [5], where $F_n[U_k(t)]$ is the Fourier coefficient of the *n*th harmonic of the time domain switching waveform *U* on the *k*th antenna element.

$$AF(\theta,t) = e^{j[\omega_c + n\omega_p]t}.\sum_{k=1}^{N} F_n[U_k(t)]\, e^{j\varphi_k} \tag{1}$$

The time modulation of the RF signal at element *k* can be represented as a series of Fourier coefficients, multiplied with harmonics of the switching frequency ω_p, then up-converted to the carrier frequency ω_c. The term $e^{j\varphi_k}$ is an element-specific phase shift, due to antenna element spacing and evaluated beam angle and can be expressed using (2), where *k* is the element number, *d* is the spacing between the elements and θ is the azimuth beam angle direction being evaluated.

$$\varphi_k = (k-1)\frac{2\pi}{\lambda}.d.sin(\theta) \tag{2}$$

In the rest of this paper we refer to the *n*th Fourier coefficient of the switching waveform *n*th harmonic, for a particular element *k,* as $Cn_k = F_n[U_k(t)]$ and the overall magnitude of the combined AF due to the *n*th harmonic as *Cn.*

Although there has been some prior research into deliberately shaping the switching waveform $U_k(t)$, such as [27], AF TMA models commonly assume an infinite slew rate on the transition of the RF signal from radiating element *k* 'on' state to element 'off' state. In this ideal case, the fundamental Fourier term $C0_k$ can be represented by (3), where T_k is the element on-time and T_p is the frame period, with $\omega_p = \frac{2\pi}{T_p}$.

$$C0_k = \frac{T_k}{T_p} \tag{3}$$

In practical systems, an RF switching ramp time of zero seconds is not achievable. Fig. 1 shows a more typical time domain waveform for *Uk(t),* with period T_p and the switch's 'on' duration time T_k, with ramping durations T_r and T_f.

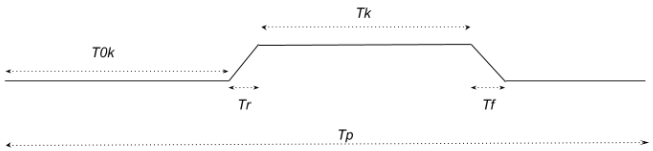

Fig. 1. *Uk(t)* example time domain form, including ramping T_r and T_f.

Next are presented the equations for the Fourier coefficients that include the effect of RF switching slew: T_r 'off-to-on' and T_f 'on-to-off' transitions. Equation (4) describes the $C0_k$ term and (5) the Cn_k term, for a particular ramped element *k* in the TMA.

$$C0_{k\_ramp} = \frac{T_r}{2T_p} + \frac{T_k}{T_p} + \frac{T_f}{2T_p} \tag{4}$$

From (4), the Fourier coefficient $C0_k$ for the *k*th element with switching slew can be seen to include the expression of the ideal (zero ramping) from (3) and additional terms associated with the ramping slew. The magnitude of the Fourier coefficient of the *n*th harmonic from the *k*th element can be predicted using (5).

$$Cn_{k\_ramp} = \left\{\frac{e^{-jn\omega_p T_{0k}}}{T_p T_r n^2 \omega_p^2}\left[e^{-jn\omega_p T_r} - 1\right] + \frac{je^{-jn\omega_p(T_{0k}+T_r)}}{2\pi n}\right\} + \left\{\frac{sin\left(\frac{n\pi T_k}{T_p}\right)}{n\pi} e^{-jn\pi\left(\frac{2T_{0k}}{T_p}+\frac{T_k}{T_p}+\frac{2T_r}{T_p}\right)}\right\} + \left\{\frac{e^{-jn\omega_p(T_{0k}+T_r+T_k)}}{n^2 2\pi\omega_p T_f}\left[1 - e^{-jn\omega_p T_f}\right] - \frac{je^{-jn\omega_p(T_{0k}+T_r+T_k)}}{2\pi n}\right\} \tag{5}$$

Hence, (4) and (5) allow the prediction of the harmonic levels as a function of switching ramp times T_r and T_f. Fig. 2 shows an example AF for a six element Dolph-Chebyshev weighted array, designed for -20dB sidelobes on the first harmonic and steering the harmonic beam to +10 degrees, with T_p set to 1µs, T_r and T_f set to 1ns (i.e. 0.1% of switching period T_p).

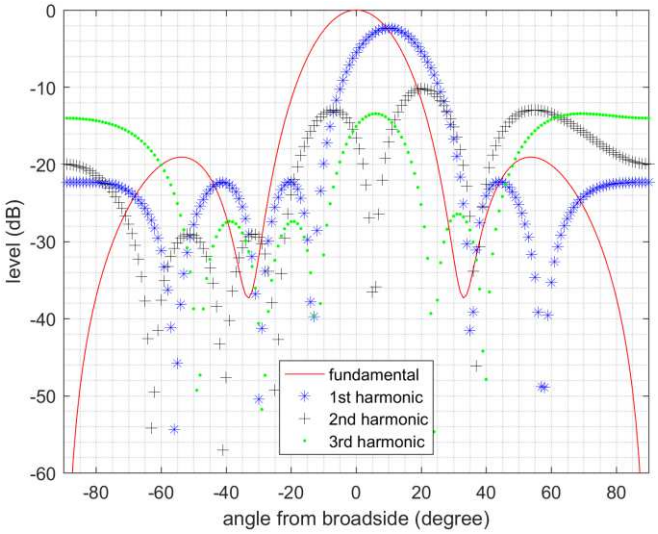

Fig. 2. Six element TMA AF for fundamental and positive harmonics 1 to 3. T_r and T_f set to 0.1% of T_p, first harmonic beam set to +10 degrees.

As an example of the effect of switching slew, let T_r and T_f now increase to 200ns (20% of T_p). As would be expected, the magnitude of the harmonic levels predicted by (5) are significantly reduced, as shown in Fig. 3.

In some circumstances it may be desirable to precisely control the magnitudes of the higher harmonic beams: control

of T_r and T_f, or adjusting T_k for a given T_r and T_f, are ways this could be achieved.

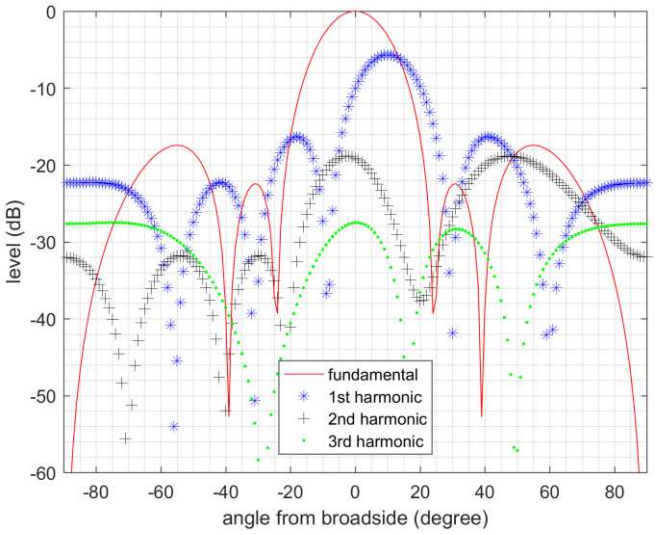

Fig. 3. Six element TMA AF for fundamental and positive harmonics 1 to 3. T_r and T_f set to 20% of T_p, first harmonic beam set to 10 degrees.

The dominant, non-steerable, beam due to Fourier *C0* component is also strongly evident in Fig. 2 and Fig. 3. This could be a limitation in using the TMA in some practical implementations, also representing a waste of energy on the non-steerable beam. We now go on to consider how the *C0* level emission may be controlled and reduced.

B. *Use of Bipolar Uk(t) to Reduce Fundamental C0 Emission*

It will be noticed from (3) that since 0 Hz coefficient *C0* can never be zero for practical array timings, there will always exist a strong emission on array boresight, which may be undesirable.

Other researchers have investigated simulated TMA techniques to control or reduce the levels of harmonics and sidelobes (often focusing on maintaining *only* the *C0* beam). Techniques usually manipulate switch timings, with use of computer optimization to reduce the sidelobe levels [29], [30], [31], [32].

In this paper we offer an alternative strategy, using dedicated simple hardware and a simple algorithm to reduce the *C0* beam, whilst also still supporting steering of other harmonic beams. One way to remove the *C0* contribution at each element is to arrange for a two-state amplifier with gains chosen such that the combined average of $U_k(t)$ over one cycle of T_p is zero. Let the *k*th element amplifier have linear gain states Ra_k (positive) and Rb_k (negative) at the antenna element. The resulting equations for the Fourier coefficients at element k in this bipolar gain scenario are shown in (6) and (7).

$$C0_k = \frac{T_k}{T_p}(Ra_k - Rb_k) + Rb_k \tag{6}$$

$$Cn_k = \left(\frac{Ra_k - Rb_k}{\pi n}\right) e^{-jn\pi\left(\frac{2T_{ok}}{T_p}+\frac{T_k}{T_p}\right)} sin\left(\frac{n\pi T_k}{T_p}\right) \tag{7}$$

If $C0_k$ is set to zero in (6), a relationship between Ra_k and Rb_k can be obtained for the *k*th element that should remove the *C0* term, as now shown in (8).

$$\frac{Ra_k}{Rb_k} = 1 - \frac{T_p}{T_k} \tag{8}$$

A simulation of the AF resulting from modified Fourier coefficients (6) and (7) to point a first harmonic beam at +10 degrees and using element specific gains Ra_k and Rb_k from (8) applied to (1) is shown in Fig. 4. (T_r and T_f are set to zero). For this simulation six antenna elements were used (k = 1..6), all Ra_k values were set to 0dB, 0 degrees phase and Rb_k values were found using (8) as follow:-

Rb1 = *Rb6* = -13.1dB, 180 degrees
Rb2 = *Rb5* = -8.1dB, 180 degrees
Rb3 = *Rb4* = 0dB, 180 degrees

Using the proposed technique, Fig. 4 clearly shows the cancellation of the fundamental *C0* emission as desired. Fig. 4 also shows visible minor effects on the shape of the remaining beams, due to the *C0* canceller, compared to the normal TMA.

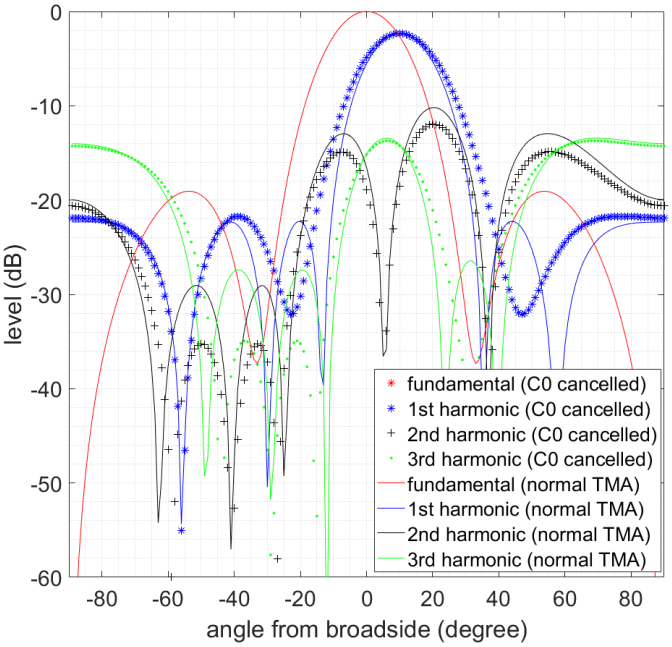

Fig. 4. Six element TMA AF for fundamental and positive harmonics 1 to 3. Harmonic beams shown for normal TMA mode and *C0* cancellation mode, first harmonic beam set to 10 degrees. Fundamental *C0* carrier component cancelled.

Key attractions of the TMA are its low cost and low implementation complexity, in contrast to using phase shifters or vector modulators commonly used in antenna arrays for beam steering. It is therefore proposed that calculating and controlling gain Rb_k and Ra_k on a per-element basis is highly unattractive, due to the complexity of element RF hardware - hence a pragmatic approach is required. The ideal values of Rb_k vary with element and desired beam angle, but we have observed that their average value across the array is constant per harmonic, regardless of the beam pointing angle.

Furthermore, we have found that all values of Rb_k can be quantized to a subset of just two values (*Rb1q*, *Rb2q*) and still provide useful (though imperfect) cancellation of the fundamental whilst steering beams in the first three harmonics. Considering the first, second and third harmonic beams, example values of *Rb1q* and *Rb2q* which led to better than 10dB *C0* cancellation across the array pattern were found by simulation and are described in linear form by (9) and (10). In (10) *mean*(*Rb*) is the average of all elements' ideal Rb_k values, as found using (8), and *Rb_mid* is the ideal value of *Rb* for the centre element in the array. *Ra* was chosen and fixed the same for all elements at 0dB.

$$Rb1q = -Ra \tag{9}$$

$$Rb2q = mean(Rb) - \frac{Rb\_mid}{6} \tag{10}$$

The choice between *Rb1q* or *Rb2q* for the gain to be used for Rb_k in element k was then made based on comparing the ideal value of Rb_k to the value *mean(Rb)* as follows:

if (Rb_k < *mean(Rb)*)
  Rb_k = *Rb1q*
else
  Rb_k = *Rb2q*
end

When pointing the second or third harmonic beam, a simpler mapping just using *Rb2q* was found sufficient: Rb_k = *Rb2q*. Further improvements in the technique to select *Rb1q* and *Rb2q* may be possible but have not been trialed, and may possibly require numerical solutions. However, the technique proposed has been sufficient to support investigation of our *C0* cancellation concept.

Example AFs using an array of six elements are shown in Fig. 5 for a first harmonic beam pointed at +18 degrees and Fig. 6 for a second harmonic beam at +35 degrees. The following Rb_k values were used for the first harmonic beam generation, using (9), (10) and the proposed *Rb1q Rb2q* algorithm:-

Rb1 = *Rb6* = -8.6dB, 180 degrees
Rb2 = *Rb5* = -8.6dB, 180 degrees
Rb4 = *Rb3* = 0dB, 180 degrees

The required values for generating *C0* reduction when pointing the second harmonic beam were:-

Rb1 = *Rb6* = -16.8dB, 180 degrees
Rb2 = *Rb5* = -16.8dB, 180 degrees
Rb4 = *Rb3* = -16.8dB, 180 degrees

Hence, it is therefore proposed that by use of RF switches and fixed gain states in the TMA, the fundamental carrier (un-steered) *C0* emission can be reduced, whilst maintaining beam steering across the remaining harmonics.

III. TMA RF Hardware Test Platform

TMAs generally requires fast RF switching, with a slew rate significantly faster than the switching frequency if higher harmonics are to be available for beams. The effect of switching slew on harmonic energy levels has been shown in (4) and (5). Furthermore, to obtain harmonic beams with a wide spectral spacing requires a high switching frequency.

To allow us to investigate our *C0* cancelling algorithm and assess the real-world performance, a 5.8GHz transmitting (TX) test platform with six novel switched antennas has been created.

A. Design of 5.8GHz RF Switching Cell and Test Platform Hardware

As described thus far, we propose to modify the TMA *Uk(t)* waveform to be bipolar, with a single fixed positive gain state (*Ra*) and two fixed negative gain states (*Rb1q*, *Rb2q*) with the same values available for use at each element. From (8) it can be seen that the ratio of stage gains are key, hence the absolute gains can be scaled to convenient practical values.

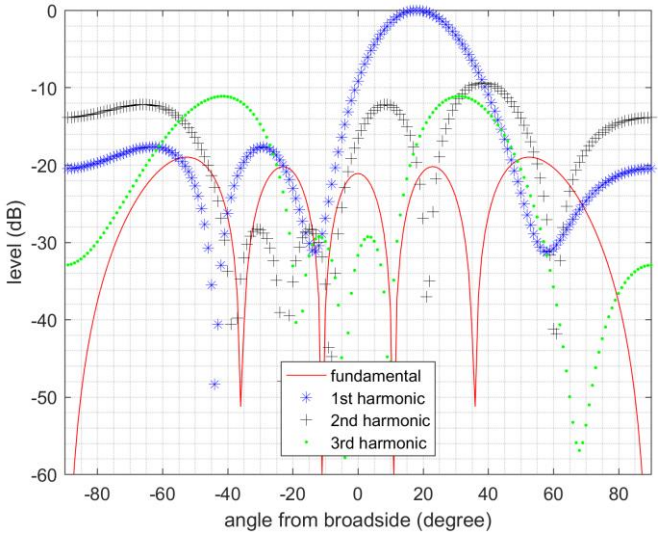

Fig. 5. Six element TMA AF for fundamental and positive harmonics 1 to 3, with first harmonic beam pointing at +18 degrees. TMA bipolar gain quantized to *Ra, Rb1q, Rb2q*. Carrier beam suppressed by 20dB.

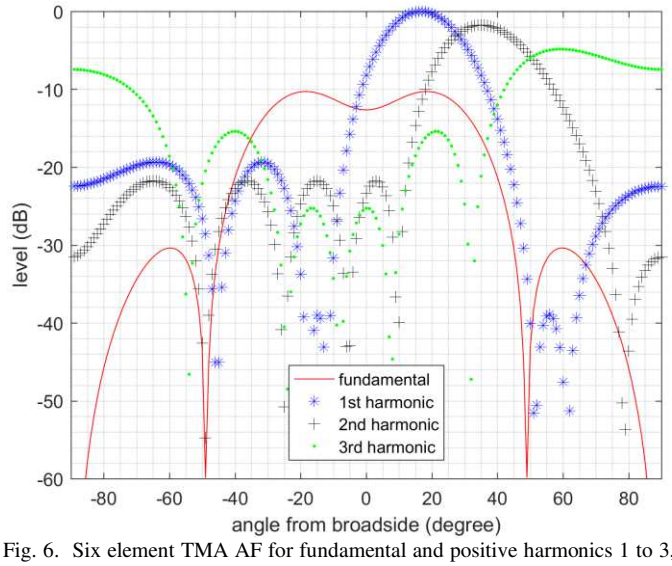

Fig. 6. Six element TMA AF for fundamental and positive harmonics 1 to 3, second harmonic beam pointing at +35 degrees. TMA bipolar gain quantized to *Ra, Rb1q, Rb2q*. Carrier beam suppressed by 10dB.

The proposed test platform consists of six identical stages (or cells), each using three gain states: *Ra* = 0dB / 0 degree phase, *Rb1q* = 0dB / 180 degree phase and *Rb2q* = -10dB / 180 degree phase. Simulations of the expected AF patterns when using the quantized gains for a desired first harmonic beam at 18 degrees are shown in Fig. 7, which shows similar AF to Fig. 5, though with further *C0* nulling on boresight.

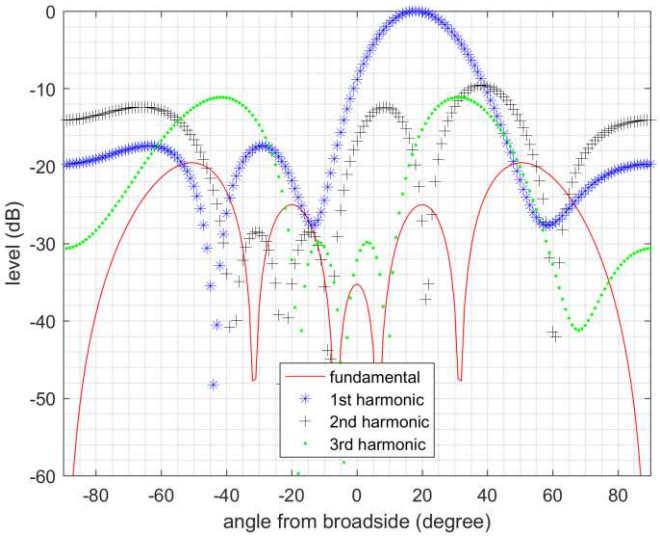

Fig. 7. Fundamental reduction for a six element array, first harmonic beam pointing at 18 degrees, fixed *Rb2q* = *Rb1q* – 10dB.

The individual cell RF hardware used to implement the required switched gains and phase is shown in Fig. 8. The single switching cell was designed based on an Analog Devices HMC7992 single pole 4-throw RF switch [33], with a resistive attenuator pad to implement level control for *Rb2q* and coplanar waveguide PCB tracking to implement the required phase inversions for *Rb1q* and *Rb2q,* with reference to *Ra*. The output of the cell branches are combined via a simple three-way Wilkinson combiner. The HMC7992 switch has the advantage of providing a 50 ohm termination to all ports, including the unselected ports. This simplifies the design of the Wilkinson output combiner network due to all ports seeing correct termination regardless of switch state. Finally, an RF amplifier using an Analog Devices ADL5611 [34] was used at the output to drive the cell's patch antenna. The switching cell was then duplicated six times to create the six element array. A six way feed network of Wilkinson splitters was created to distribute the input 5.8GHz RF signal to all the cells.

The switching control and sequencer for the TMA was implemented using a Microchip DSPIC (DSPIC33EP512GP806) [35], clocked internally at 140MHz and providing a sample rate of 2Msamples/s in the form of a 12 bit parallel word to control switch states for all the HMC7992 switches. The DSPIC hence defines the overall frame length T_p, as well as T_k and T_{0k}. The DSPIC produces 70 discrete samples per each frame, resulting in a T_p of 35µs. Fig. 9 shows the structure of the complete system, including RF input signal distribution.

The completed PCB consists of an FR4 substrate 1.6mm thick with two copper layers and with an overall PCB size of 210mm by 160mm. The radiating elements are conventional 5.8GHz patch antennas, with centre spacing of 19mm.

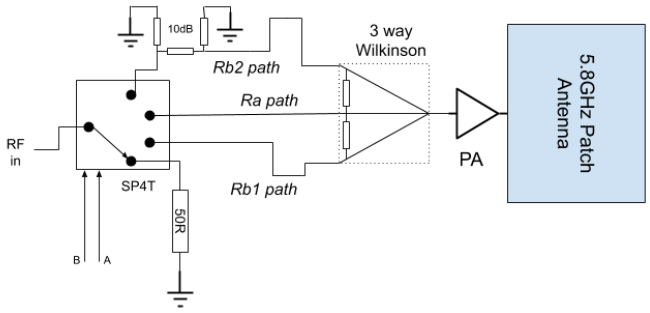

Fig. 8. A single TMA cell with *Ra*, *Rb1q* and *Rb2q* paths selected by RF switch.

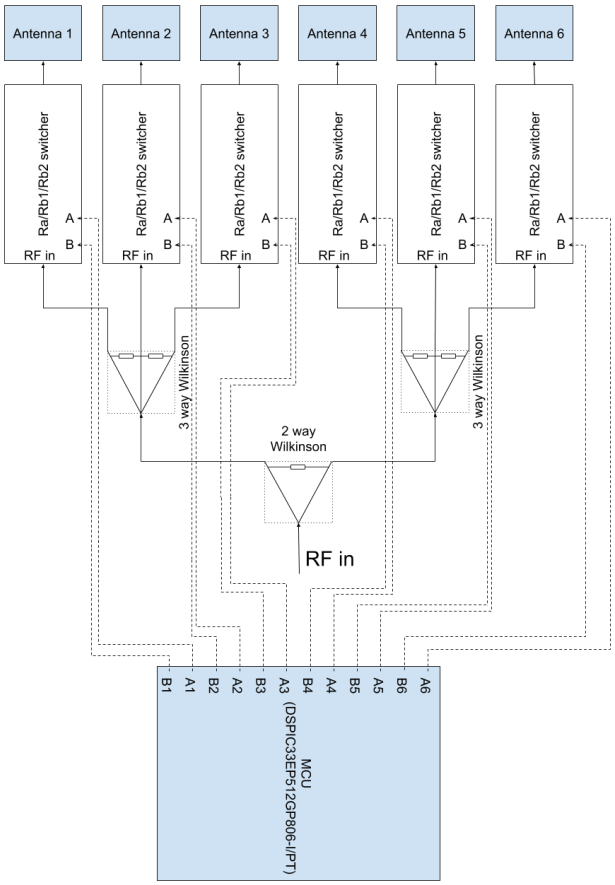

Fig. 9. Full TMA RF hardware system, using six stages and DSPIC MCU pattern sequencer.

B. Generation of Switching Patterns for TMA Hardware Platform

Trial switching patterns were generated in Matlab and then loaded into the DSPIC. The switching patterns were created using (1) and (2) to obtain a chosen *n* harmonic beam to point in a desired angular direction. The AF for the array with particular element timings can therefore be expressed by (11).

$$AF(\theta,t) = e^{j[\omega_c + n.\omega_p]t}.\sum_{k=1}^{N} e^{j\varphi_k}.\frac{sin\left(n.\pi\frac{T_k}{T_p}\right)}{n.\pi}.e^{-jn\pi\left(2\frac{T_{0k}}{T_p}+\frac{T_k}{T_p}\right)} \quad (11)$$

The derivation of equations used to calculate the element-specific timings T_k and T_{0k} for a particular frame period T_p are based on the approach in [5], but now extended here to use an arbitrary desired harmonic n, as shown in (12) and (13).

$$T_k = T_p.\frac{arcsin(G(k))}{n.\pi} \quad (12)$$

$$T_{0k} = T_p.\left[\frac{(k-1)d_\lambda sin(\theta_t)}{n} - \frac{T_k}{2T_P}\right] \quad (13)$$

In (12) and (13), *G()* is a desired Dolph-Chebyshev array of weights for the overall array pattern [36], n is the desired harmonic beam (1 for first harmonic, 2 for second, etc) to point in desired angular direction θ_t, and d_λ is the element spacing divided by wavelength (0.5 used for half-wavelength spaced elements). Dolph-Chebyshev array weights were chosen to achieve a 20dB sidelobe level.

The *maximum* beam steering angle possible for a particular harmonic can be defined as the point when any of the array's RF switches have an on time (T_{0k} + T_k) exceeding the frame period T_p. Such an occurrence would cause the switch to be turned off after the end of the current frame duration – which is clearly an invalid configuration. For our system, the steering range is –19 degrees to +19 degrees for the first harmonic and –46 degrees to +46 degrees for the second harmonic.

It should also be noted that the expected array gain for the harmonic beam from (1) and (7) can be calculated and compared for different Rb_k values, including the conventional TMA with no *C0* cancelation (i.e. Rb_k equals zero).

C. Initial Testing of TMA Hardware Platform

The built TMA PCB was first tested using 5.8GHz conducted RF signals feeding each cell, to test their phase and amplitude alignments. The results of this commissioning test are shown in Table I, overall showing good agreement with the desired amplitude and phase shifts required for *Ra*, *Rb1q* and *Rb2q* for each cell. The expected conducted gain for the *Ra* path was -4dB (due to FR4 PCB tracking, Wilkinson splitters, etc) and the mean *Ra* path gain measured was -6dB. When combined with a typical patch antenna gain, this leads to a predicted element cell radiated gain of circa -3dBi.

The typical measured RF power ramp duration T_f was 90ns and the T_r duration was 100ns, as measured using a Rohde & Schwarz FSIQ26 spectrum analyser in 0 Hz mode. Given our T_p of 35µs and (5) suggests that the RF switches will not enforce notable attenuation on the harmonic beams.

The measured mean gain difference between *Rb1q* and *Ra* paths was -0.6dB and the mean gain difference between *Rb2q* and *Ra* paths was -10.3dB. The mean phase error for the required 180 degree shift between *Rb1q* and *Ra* paths was -0.2 degrees and for *Rb2q* to *Ra* paths was 1.0 degree. This overall gave confidence that the TMA system was functioning adequately and absolute gain and phase alignment between cell stages was acceptable.

The return loss and coupling between the 5.8GHz patch antennas was also measured. The return loss for each antenna was found to be better than 10dB and the isolation due to mutual coupling was better than 13dB between adjacent elements.

Simulations were run to investigate the expected performance of the cancellation algorithm when using the measured PCB values for all elements' *Ra*, *Rb1q* and *Rb2q*. Fig. 10 shows the expected AF for the carrier fundamental and first harmonic beam when pointed at +18 degrees; still providing 20dB of rejection relative to the carrier, as also seen in Fig. 5.

TABLE I
MEASURED CELL STAGE GAINS AND PHASE SHIFTS

Stage *k*	Gain Delta *Rb1q(k)-Ra(k)* (dB)	Gain Delta *Rb2q(k)-Ra(k)* (dB)	Phase Delta *Rb1q(k)-Ra(k)* (degrees)	Phase Delta *Rb2q(k)-Ra(k)* (degrees)
1	-2.4	-10.4	-179	-180
2	2.3	-10	-173	-178
3	0.3	-9.5	-187	-180
4	-1	-10	-180	-181
5	-1	-10.6	-182	-181
6	-1.6	-11.2	-180	-174

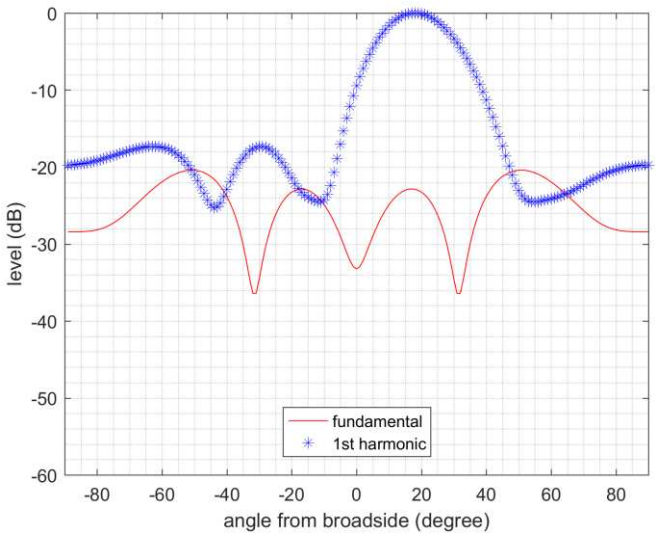

Fig. 10. Six element TMA simulated AF for fundamental and first positive harmonic. Harmonic beam pointing at +18 degrees. TMA bipolar gain quantized to measured PCB values for *Ra, Rb1q, Rb2q*. Fundamental suppressed by 20dB.

IV. TMA Radiated Chamber Tests

The TMA PCB was tested in an anechoic chamber in the University of Sheffield's Communications Research Group. Tests evaluated the magnitude of the fundamental (*C0*), first (*C1*) and second (*C2*) harmonic beam patterns. The measurement system consisted of a Gigatronics 2540B 5.8GHz CW signal source, Rohde & Schwarz FSV40-N Spectrum Analyser and AEL H-1498 measurement horn antenna. The H-1498 measurement antenna was mounted on a

movable arch, pointing down vertically from above towards the TMA under test, thus allowing measurement of the radiated energy at various azimuth angles (test PCB facing upwards). Due to limitations of the measurement system, one measurement horn was used to measure emissions for clockwise rotations of the arch and another identical horn for anti-clockwise rotation. The measurement system is shown in Fig. 11, with an example measurement shown in Fig. 12a. Fig. 12b shows the RF side of the assembled TMA PCB. The distance d between the measurement horn(s) and the TMA PCB was 56cm. Since this is an anechoic measurement environment and far-field, simple free space path loss (FSPL) can be used at the measurement wavelength λ, using (14).

$$\mathrm{FSPL} = 20\log_{10}\left(\frac{4\pi d}{\lambda}\right) \mathrm{dB} \quad (14)$$

The manufacturer's specification of the H-1498 horn antenna gain (circa 8dBi), a calculation of 43dB for the FSPL between the TMA PCB and measurement horn and a measurement of the overall cable loss allowed an estimation of the radiating gain of the TMA as an antenna array system to be made. Therefore, the measurement figures in this section show the measured radiated gain in dBi, after accounting for the measurement losses in the system. This is useful in allowing an absolute comparison between various radiated levels and also comparing to theoretical simulations. Background noise was circa 70dB below measured main-lobe powers.

Tests were first performed without any screening can fitted to the PCB and with a desired *C1* first harmonic beam steered to +18 degrees, first without and then with the *C0* cancellation algorithms operational, with results shown in Fig. 13 and Fig. 14 respectively. Since, at this stage, no RF screening enclosure was fitted to the PCB, the reduction in achieved *C0* cancellation was suspected to be due to radiation directly from the circuitry, prior to the patch antennas, thus limiting the dynamic range of the chamber measurements. To investigate this, the outputs from each TX stage were terminated in 50 ohm loads and their antennas isolated. The emissions emanating from the board were then measured and indeed confirmed to be significant. The effect of this leakage from the PCB (mainly from the input Wilkinson distribution network) was characterised and found to impose a measurement floor to the antenna gain calculations, as presented in Table II.

TABLE II
GAIN MEASUREMENT FLOOR DUE TO PCB LEAKAGE EMISSIONS

Measurement angle (degrees)	Fundamental (*C0*) measurement floor (dBi)	1st harmonic (*C1*) measurement floor (dBi)	2nd harmonic (*C2*) measurement floor (dBi)
0	-10	-30	-28
-10 / +10	-10	-30	-44
-20 / +20	-20	-40	-37
-40 / +40	-20	-33	-37

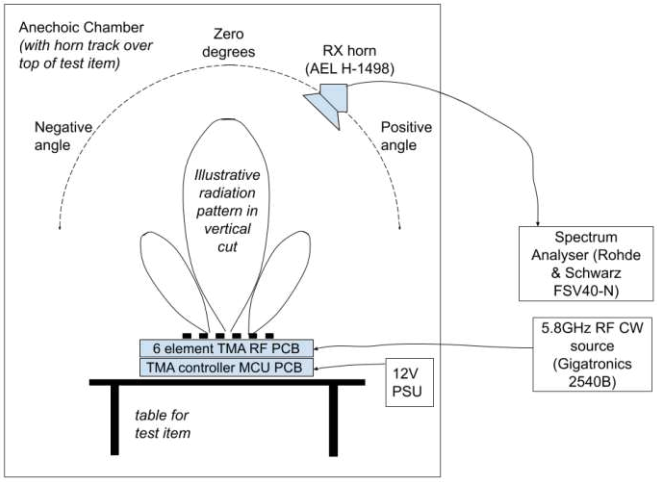

Fig. 11. Laboratory TMA radiated measurement system.

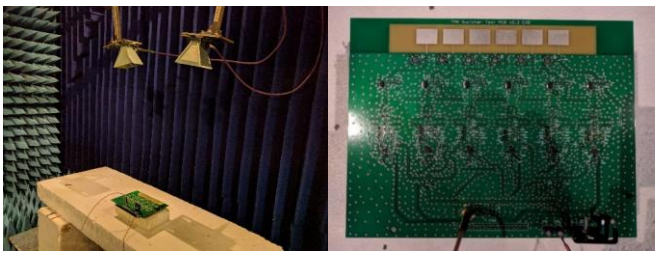

(a) (b)

Fig. 12. TMA RF hardware testing. (a) example TMA pattern measurement being taken, (b) built TMA test system, with DSPIC on reverse of PCB.

To help reduce the compromising of the measurements due to carrier leakage, a screening can was then fitted over the entire RF circuitry. Tests were again performed with a desired *C1* first harmonic beam steered to +18 degrees, without and then with the *C0* cancellation algorithms operational, with results shown in Fig. 15 and Fig. 16 respectively. Comparing the *C0* traces on Fig. 14 and Fig. 16 shows a circa 5dB reduction in carrier seen on the boresight, confirming that PCB leakage had been an issue. Figs. 14 and 16 also show the predicted theoretical radiated gain (isotropic reference) of the array from (11), for comparison. Unless stated, all subsequent reported measurements are using the screened PCB system.

Tests were then performed for a desired *C1* harmonic beam steered to -18 degrees both without and with the *C0* cancellation algorithms operational, with results shown in Fig. 17 and Fig. 18 respectively. In all cases the *C0* magnitude is reduced on boresight by our technique and the main lobe of the *C1* steered beam broadly follows the gain and beam shape from the AF predictions.

Comparing Fig. 15 to Fig. 16 also shows an increase in the desired first harmonic *C1* beam. However Fig. 16 appears to also show circa 5dB less than expected *C0* cancellation was achieved on the PCB, for reasons we discuss later.

The TMA was then configured to produce a desired beam at +35 degrees, using the second switching harmonic, *C2*. The results for this scenario when the fundamental *C0* signal is present unmodified and then when the *C0* canceller is operational are shown in Fig. 19 and Fig. 20 respectively.

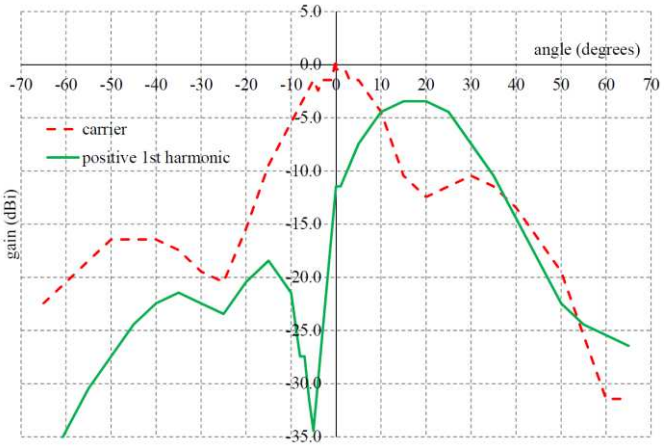

Fig. 13. Measured radiated gain of TMA when pointing first positive harmonic beam to +18 degrees in conventional TMA pattern operation (no PCB screening can).

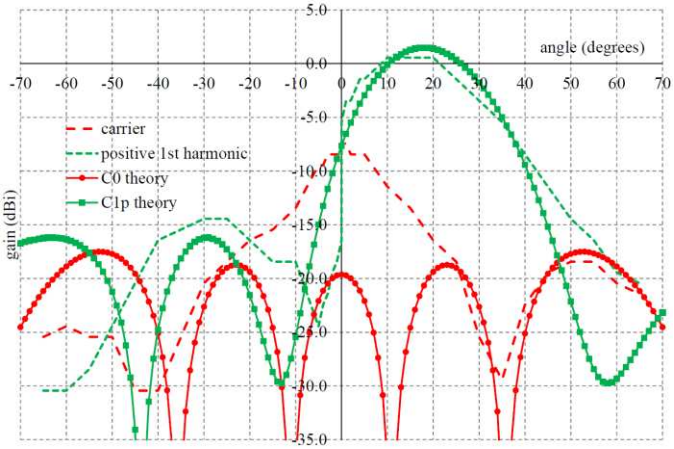

Fig. 14. Measured radiated gain of TMA pointing first positive harmonic beam to +18 degrees with *C0* canceller activated (no PCB screening can).

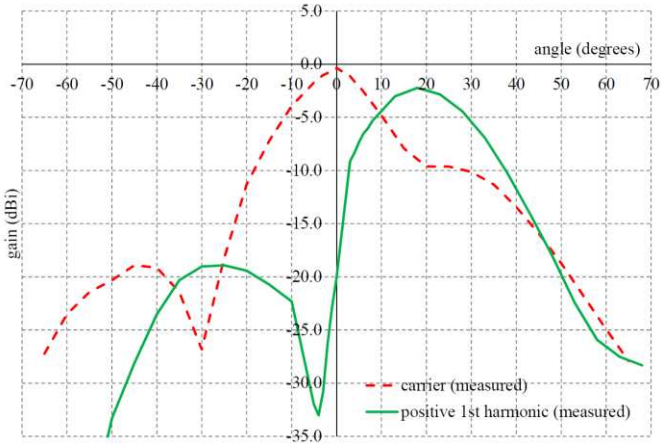

Fig. 15. Measured radiated gain of TMA when pointing first positive harmonic beam to +18 degrees in conventional TMA pattern operation (with PCB screening can).

In Fig. 20 the level of cancellation of the *C0* beam is less than that obtained when steering the first harmonic beam, such as in Fig. 16. This is expected and due to the compromise made in quantizing element gains Rb_k and Ra_k to common *Ra*, *Rb1q* and *Rb2q* fixed gain states, as discussed in Section IIB. Improved *C0* cancellation would require either more *Rb* states or variable control of gains Rb_k and Ra_k per element.

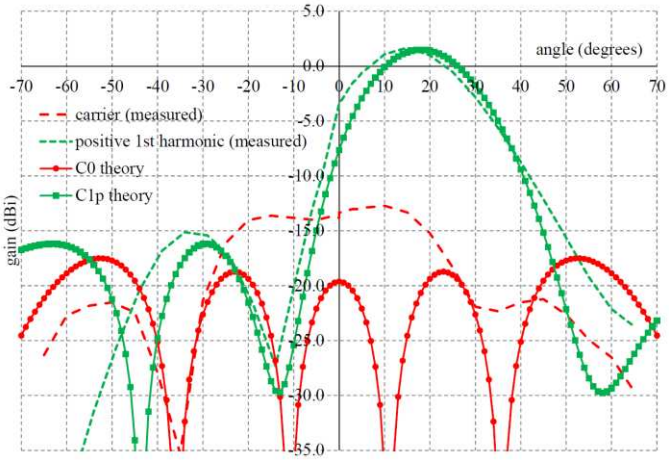

Fig. 16. Measured radiated gain of TMA pointing first positive harmonic beam to +18 degrees with *C0* canceller activated (with PCB screening can).

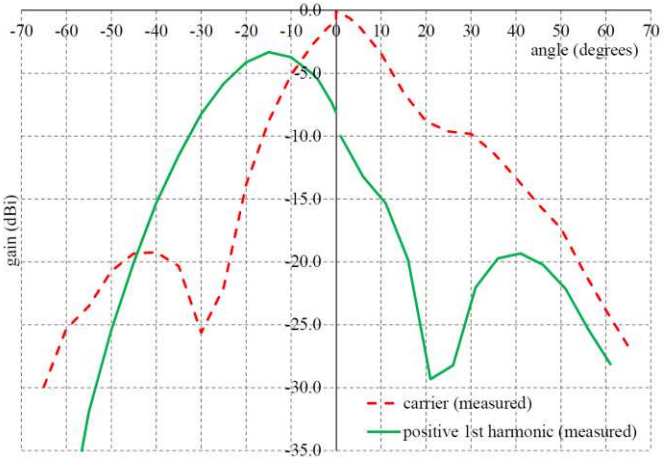

Fig. 17. Measured radiated gain of TMA pointing first positive harmonic beam to -18 degrees in conventional TMA pattern operation (with PCB screening can).

Comparing Fig. 19 and Fig. 20 does show that the fundamental emission on boresight due to *C0* has been reduced by circa 10dB and the beam pattern also follows the trend predicted in AF simulations. The wanted *C2* emission has increased and also closely follows AF simulations.

To allow comparisons, the *C2* and *C0* emissions without the screening can fitted are shown in Fig. 21. An improvement in *C0* cancelation due to the screening can is seen in Fig. 20, also showing a close trend to theoretical predictions for *C0*.

With the screening can refitted, the TMA was then configured to produce a desired *C2* beam at -35 degrees, again using the second harmonic. The results for this scenario when the fundamental *C0* signal is present and then when the *C0* canceller is operational are shown in Fig. 22 and Fig. 23 respectively.

Note that Figs. 16, 18, 20, 21 and 23 also show the predicted gain (isotropic reference) of the array from (11), for comparison. Here, the predicted gain of (11) uses actual PCB

measured values for *Ra*, *Rb1q* and *Rb2q,* extracted from each of the six cells.

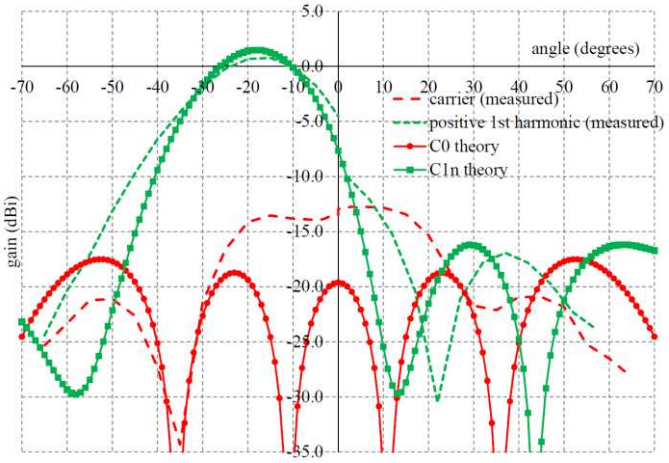

Fig. 18. Measured radiated gain of TMA pointing first positive harmonic beam to -18 degrees with *C0* canceller activated (with PCB screening can).

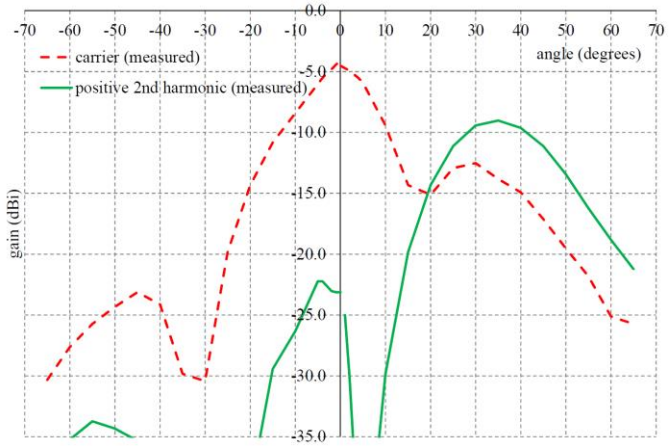

Fig. 19. Measured radiated gain of TMA pointing second positive harmonic beam to +35 degrees in conventional TMA pattern operation (with PCB screening can).

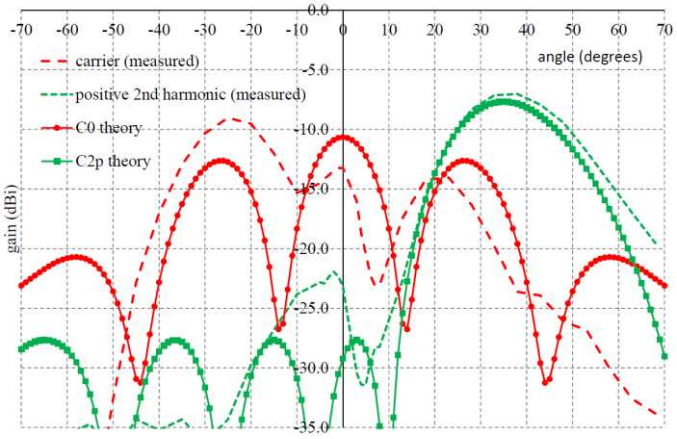

Fig. 20. Measured radiated gain of TMA pointing second positive harmonic beam to +35 degrees with *C0* canceller activated (with PCB screening can).

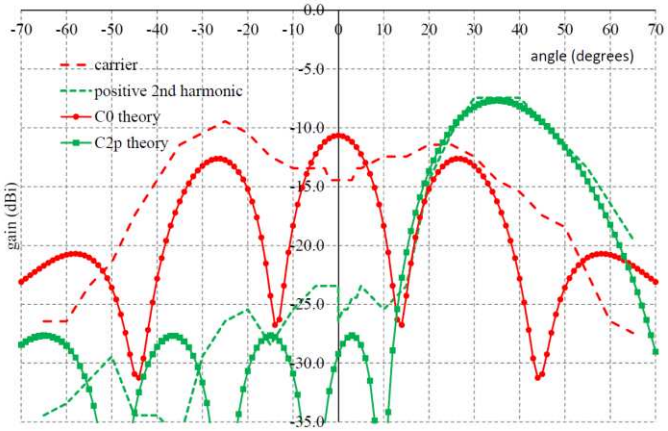

Fig. 21. Measured radiated gain of TMA pointing second positive harmonic beam to +35 degrees with *C0* canceller activated (no PCB screening can).

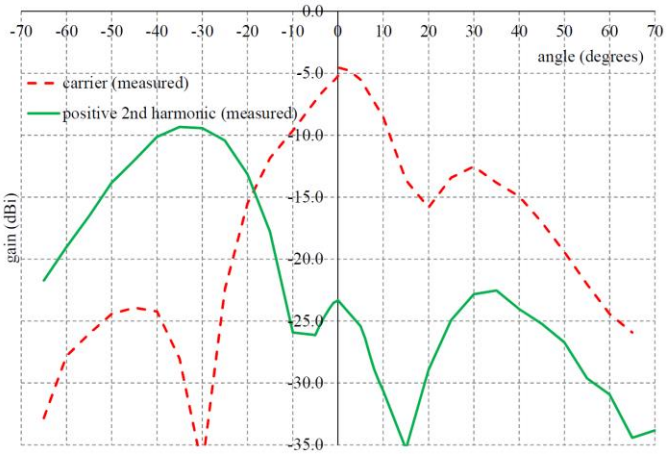

Fig. 22. Measured radiated gain of TMA pointing second positive harmonic beam to -35 degrees in conventional TMA pattern operation (with PCB screening can).

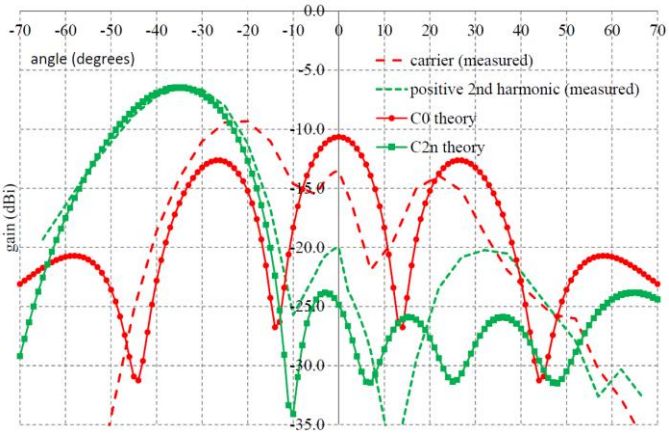

Fig. 23. Measured radiated gain of TMA pointing second positive harmonic beam to -35 degrees with *C0* canceller activated (with PCB screening can).

From Fig. 22 and Fig. 23 it is clear that the *C0* canceller is reducing the strength of the fundamental emission on boresight by circa 8dB and also following the trend predicted by the AF simulations. Similarly, the desired *C2* beamwidth and gain are closely matching AF calculations and the performance is also broadly similar to the AF as seen in Fig. 20 (using the opposite beam).

The fundamental radiated performance of three antennas and associated circuit cells (A1, A3, A6) within the array was also characterised, to investigate their basic patterns, with results shown in Fig. 24. The expected radiated gain of a cell is -3dBi (based on measured average *Ra* gain of -6dB, a theoretical PCB patch antenna directivity of 6dBi and FR4 radiating efficiency of -3dB) - which agrees well with the boresight gains measured for A1, A3 and A6. The radiated RF leakage without DC power applied is also shown in Fig. 24. It is clear that whilst there are some differences between the individual measured antenna cells (contributed to by the spread in *Ra* circuit performance as well as possible antenna radiating pattern differences), the patterns are still broadly similar. The leakage from the PCB without DC power applied is also evident and imposes a fundamental floor on radiated *C0* boresight cancellation of circa -18dBi. From subsequent tests we have found that RF radiation from the feed coax close to the PCB SMA connector, and the use of spot-solder joints (rather than seam solder joints) around the screening can are both still leading to some higher than desired carrier leakage.

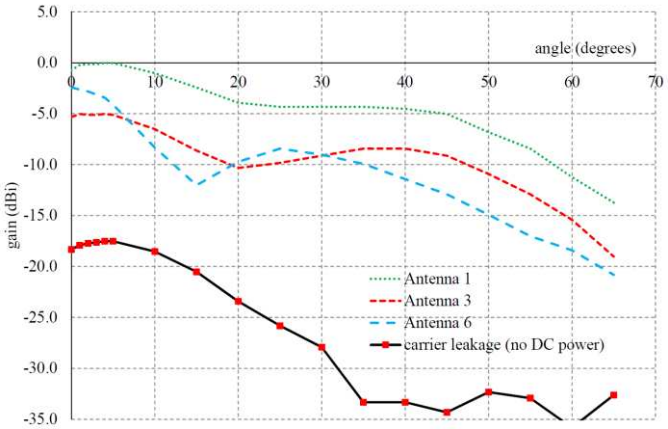

Fig. 24. Measured radiated gain pattern (half of pattern) for three TMA antenna cells (*Ra* path and a single antenna tested in turn, all other antennas off). Carrier leakage with PCB unpowered is also shown.

The reduction of the *C0* beam can be predicted using (6). With the actual PCB values used for *Rb1q*, *Rb2q*, *Ra* and chosen switch timings, we would expect to see 20dB reduction in the *C0* emission, when using the 18 degree *C1* harmonic beam. We would expect to see a 10.6dB reduction in *C0* emission when using the 35 degree *C2* harmonic beam. However, the measured *C0* reduction is 12.6dB when the 18 degree first harmonic beam is selected and worst-case 5dB (9.1dB when only considering *C0* at boresight) when the 35 degree second harmonic beam is selected. Fig. 24 suggests that the unwanted PCB emissions from carrier leakage could be limiting the performance of the *C0* cancellation, as observed in Fig. 16, Fig. 18, Fig. 20 and Fig. 23.

Also, note that due to the choice of values made for *Rb1q*, *Rb2q* and *Ra,* the existing PCB design is theoretically, and in practice, more suited to *C0* cancellation when pointing the *C1* beam, rather than when using the *C2* beam. This difference can, for example, be seen by comparing Fig. 16 and Fig. 20 or indeed Fig. 5 and Fig. 6.

It is interesting to note that when the *C0* reduction algorithm is operational, as well as attenuating the radiated energy in the boresight *C0* beam, there is also an increase in energy in the harmonic beams. This can be predicted using (7) using the actual timings and *Ra, Rb1q* and *Rb2q* values obtained from the PCB. The expected gain enhancement of the first harmonic beam is 4.1dB and for the second harmonic beam an enhancement of 2.3dB is expected. In practice we see an enhancement of 3.9dB for the first harmonic and 2.8dB for the second harmonic beam.

Overall, with the limitations of the PCB as-built, we are achieving an effective decrease in *C0* emission of 16.5dB relative to the first harmonic beam *C1*, which from theory should be 21.3dB if *C0* RF PCB leakages were insignificant. We achieve a decrease in effective *C0* emission of worst-case 7.6dB (11.8dB if only *C0* boresight is considered) relative to the second harmonic beam *C2*, which broadly agrees with the theoretical prediction of 10.8dB.

The measured equivalent isotropic gain of the *C0* cancelled TMA system is +2dBi for the first harmonic beam and -6dBi for the second harmonic beam. A comparable phased array (using the same PCB RF amplifiers, splitters and antennas, but assuming phase shifters are used instead of the TMA RF switches) would be expected to have a gain of +4.6dBi. The 2.6dB loss in first harmonic beam gain can be considered an *implementation loss* for the TMA. Such a loss may be acceptable for many applications, given the lower cost of the hardware and simpler digital control supported, possibly also mitigated by using a larger array of elements.

V. Conclusion

This paper has presented new TMA techniques to predict and control the magnitude of the fundamental carrier (*C0*) beam whilst still steering higher-order radiated harmonic beams (*C1*, *C2*). These techniques will enable TMA system to become more useful to industrial and commercial radio system designers.

The algorithmic concepts have been demonstrated and tested using a new, bespoke, RF hardware platform operating at 5.8GHz, with test results generally showing good agreement with theory. The sensitivity of the TMA radiated performance to PCB RF leakage emissions has been identified as a limiting factor.

Further work is now planned to operate the TMA platform at higher switching rates and to develop techniques to control multiple harmonic beam levels. For this we are developing an FPGA platform to control the TMA, replacing the DSPIC. This faster switching platform will then allow us to investigate further harmonic control, such as using pulse-splitting techniques as investigated in [37]. Higher switching rates are vital to spectrally separate the generated harmonics, thus supporting transport of user modulated data on an RF channel. The higher switching rates will also allow us to vary T_k as a means to control harmonic levels using (5) in systems where T_r and T_f are fixed, which is the usual case for RF switches.

There is currently much interest in beam steering for future

5G and mmWave mobile systems. To be commercially viable, such systems must be cost-effective and very power efficient. The simple and low cost RF hardware TMA concepts described in this paper may be applicable to such future handset antenna arrays, which could be pointing traffic to only a single base station at a given instant.

Although this paper has focused on a transmitter TMA, the concept of the triple-gain-state RF switch circuitry could also be applied for receiving arrays using low noise amplifiers, or indeed in a transceiver array.

REFERENCES

[1] S. Kutty, and D. Sen, "Beamforming for millimeter wave communications: an inclusive survey," *IEEE Communications Surveys & Tutorials,* vol. 18, no. 2, pp. 949-973, Dec. 2015.

[2] W. H. Kummer, A. T. Villeneuve, T. S. Fong, and F. G. Terrio, "Ultra-low sidelobes from time-modulated arrays," *IEEE Transactions on Antennas and Propagation,* vol. 11, no. 6, pp. 633-639, Nov. 1963.

[3] Y. Tong, and A. Tennant, "Simultaneous control of sidelobe level and harmonic beam steering in time-modulated linear arrays," *Electronics Letters,* vol. 46, no. 3, pp. 201-202, Feb. 2010.

[4] W-Q. Wang, H. C. So, and A. Farina, "An overview on time/frequency modulated array processing," *IEEE Journal of Selected Topics in Signal Processing,* vol. 11, no. 2, pp. 228-246, March, 2017.

[5] G. Li, S. Yang, Y. Chen, and Z. Nie, "A novel beam scanning technique in time modulated linear arrays," *2009 IEEE Antennas and Propagation Society International Symposium,* Charleston, 2009, pp. 1-4.

[6] P. Rocca, G. Oliveri, R. J. Mailloux, and A. Massa, "Unconventional phased array architecture and design methodologies - a review," *Proceedings of the IEEE,* vol. 104, no. 3, pp. 544-560, March, 2016.

[7] Y. Tong, and A. Tennant, "A two-channel time modulated linear array with adaptive beamforming," *IEEE Transactions on Antennas and Propagation,* vol. 60, no. 1, pp. 141-147, Jan. 2012.

[8] E. T. Bekele, L. Poli, L. Manica, P. Rocca, A. Massa, S. Yang, and Q. Zhou, "Advances on time-modulated arrays for cognitive radio," *7th European Conference on Antennas and Propagation (EuCAP),* Gothenburg, 2013, pp. 344-346.

[9] W. C. Barott, and S. Fucharoeb, "Experimental time-modulated beamformer for interference mitigation in a radio spectrometer," *IEEE Journal of Selected Topics in Signal Processing,* vol. 11, no. 2, pp. 271-281, March, 2017.

[10] L. Poli, P. Rocca, G. Oliveri, and A. Massa, "Adaptive nulling in time-modulated linear arrays with minimum power losses," *IET Microwaves, Antennas & Propagation,* vol. 5, no. 2, pp. 157-166, January, 2011.

[11] G. Bogdan, M. Jarzynka, and Y. Yashchyshyn, "Experimental study of signal reception by means of time-modulated antenna array," *21st International Conference on Microwave, Radar and Wireless Communications (MIKON),* Krakow, 2016, pp. 1-4.

[12] G. Bogdan, Y. Yashchyshyn, and M. Jarzynka, "Time-modulated antenna array with lossless switching network," *IEEE Antennas and Wireless Propagation Electronics Letters,* vol. 15, pp. 1827-1830, March, 2016.

[13] J. Chen, R. Jin, H. Fan, J. Geng, X. Liang, and C. He, "Wideband direction-finding based on time-modulated antenna arrays," *IEEE 4th Asia-Pacific Conference on Antennas and Propagation (APCAP),* Kuta, 2015, pp. 48-49.

[14] A. O'Donnell, W. Clark IV, J. Ernst, and R. McGwier, "Analysis of modulated signals for direction finding using time modulated arrays," *IEEE Radar Conference (RadarConf),* Philadelphia, 2016, pp. 1-5.

[15] D. Ni, S. Yang, Y. Chen, and J. Guo, "A study on the application of subarrayed time-modulated arrays to MIMO radar," *IEEE Antennas and Wireless Propagation Letters,* vol. 16, pp. 1171-1174, November, 2017.

[16] G. Li, S. Yang, and Z. Nie, "A study on the application of time modulated antenna arrays to airborne pulsed doppler radar," *IEEE Transactions on Antennas and Propagation,* vol. 57, no. 5, pp. 1578-1582, May, 2009.

[17] J. Euzière, R. Guinvarc'h, M. Lesturgie, B. Uguen, and R. Gillard, "Dual function radar communication time-modulated array," *2014 International Radar Conference,* Lille, 2014, pp. 1-4.

[18] J. Euzière, R. Guinvarc'h, I. Hinostroza, B. Uguen, and R. Gillard, "Time modulated array for dual function radar and communications," *IEEE International Symposium on Antennas and Propagation & USNC/URSI National Radio Science Meeting,* Vancouver, 2015, pp. 806-807.

[19] J. Euzière, R. Guinvarc'h, and I. Hinostoza, "Optimizing communications in TMA for radar," *IEEE International Symposium on Antennas and Propagation (APSURSI),* Fajardo, 2016, pp. 705-706.

[20] Y. Wang, and A. Tennant, "Experimental time-modulated reflector array," *IEEE Transactions on Antennas and Propagation,* vol. 62, no. 12, pp. 6533-6536, December, 2014.

[21] R. Maneiro-Catoira, J. Brégains, J. A. García-Naya, L. Castedo, P. Rocca, and L. Poli, "Performance analysis of time-modulated arrays for the angle diversity reception of digital linear modulated signals," *IEEE Journal of Selected Topics in Signal Processing,* vol. 11, no. 2, pp. 247-258, March, 2017.

[22] L. Poli, P. Rocca, G. Oliveri, and A. Massa, "Harmonic beamforming in time-modulated linear arrays," *IEEE Transactions on Antennas and Propagation,* vol. 59, no. 7, pp. 2538-2545, July, 2011.

[23] A. Tennant, and B. Allen, "Generation of OAM radio waves using circular time-switched array antenna," *Electronics Letters,* vol. 48, no. 21, pp. 1365-1366, October, 2012.

[24] C. Sun, S. Yang, and Y. Chen, "Generation of orbital angular momentum (OAM) waves using time-modulated circular arrays," *IEEE International Workshop on Electromagnetics: Applications and Student Innovation Competition (iWEM),* Nanjing, 2016, pp. 1-2.

[25] A. Reyna, L. I. Balderas, and M. A. Panduro, "Time-modulated antenna arrays for circularly polarized shaped beam patterns," *IEEE Antennas and Wireless Propagation Letters,* vol. 16, pp. 1537-1540, January, 2017.

[26] R. Maneiro-Catoira, J. Brégains, J. A. García-Naya, and L. Castedo, "Enhanced time-modulated arrays for harmonic beamforming," *IEEE Journal of Selected Topics in Signal Processing,* vol. 11, no. 2, pp. 259-270, March, 2017.

[27] E. T. Bekele, L. Poli, P. Rocca, M. D'Urso, and A. Massa, "Pulse-Shaping Strategy for Time Modulated Arrays - Analysis and Design," *IEEE Transactions on Antennas and Propagation,* vol. 61, no. 7, pp. 3525-3537, July, 2013.

[28] P. Rocca, L. Poli, and A. Massa, "Instantaneous directivity optimisation in time-modulated array receivers," *IET Microwaves, Antennas & Propagation,* vol. 6, pp. 1590-1597, November, 2012.

[29] P. Rocca, and A. Massa, "Innovative Approaches for optimized Performance in Time-Modulated Linear Arrays," *Antennas and Propagation Society International Symposium,* Charleston, 2009, pp. 1-4.

[30] L. Poli, P. Rocca, and A. Massa, "Beam pattern optimization in time-modulated linear arrays," *IEEE International Symposium on Phased Array Systems and Technology,* Waltham, 2010, pp. 876-878.

[31] S. Yang, Y. B. Gan, and A. Qing, "Sideband suppression in time-modulated linear arrays by differential evolution algorithm," *IEEE Antennas and Wireless Propagation Letters,* vol. 1, pp. 173-175, 2002.

[32] L. Poli, P. Rocca, L. Manica, and A. Massa, "Handling sideband radiations in time-modulated arrays through particle swarm optimization," *IEEE Transactions on Antennas and Propagation,* vol. 58, no. 4, pp. 1408-1411, April, 2010.

[33] Analog Devices Ltd HMC7992 datasheet Available: https://www.analog.com/en/products/hmc7992.html

[34] Analog Devices Ltd ADL5611 datasheet Available: https://www.analog.com/en/products/adl5611.html

[35] Microchip Semiconductors Ltd dsPIC33EP512GP806 datasheet Available: https://www.microchip.com/wwwproducts/en/dsPIC33EP512GP806

[36] C. A. Balanis, "Chapter 6", in *Antenna Theory - Analysis and Design.* 3rd ed. New Jersey, Wiley-Interscience, 2005.

[37] L. Poli, P. Rocca, F. Viani, and A. Massa, "Advanced harmonic radiations design in time-modulated antenna arrays," *2015 IEEE International Symposium on Antennas and Propagation & USNC/URSI National Radio Science Meeting*, Vancouver, 2015, pp. 812-813.

Edward A. Ball (M 2008–present) Edward (Eddie) became a Member of IEEE in April 2008 and was born in Blackpool, United Kingdom in November 1973. Eddie graduated in 1996 with a 1st Class Master of Engineering Degree in Electronic Systems Engineering, from the University of York, York, United Kingdom.

After graduating, he worked in industry for 20 years, first spending 15 years working as Engineer, Senior RF Engineer and finally Principal RF Engineer at Cambridge Consultants Ltd in Cambridge, UK. He then spent 5 years as Principal RF Engineer and Radio Systems Architect at Tunstall Healthcare Ltd in Whitley, UK. In November 2015 he joined the Department of Electronic and Electrical Engineering at the University of Sheffield, Sheffield, United Kingdom, where he now works as Reader in RF Engineering. His research interests cover all areas of radio technology, from RF system design, RF circuit design (sub-GHz to mm-wave) and the application of radio technology to real-world industrial and commercial problems. He has a particular passion for RF hardware design.

Mr. Ball is a member of the IET and is a Chartered Engineer.

Alan Tennant (M 1992-present) received the B.Eng. degree in Electronic Engineering and Ph.D. degree in Microwave Engineering from the University of Sheffield, Sheffield, U.K., in 1985 and 1992, respectively.

Previously, he was with BAE Systems, Stevenage, U.K. He then joined DERA, where he worked on phased-array antenna systems before taking up an academic post with Hull University, Hull, U.K. He returned to Sheffield University in 2001 as a Senior Lecturer with the Communications and Radar Group and is now Professor, where he is involved in research into techniques, materials, and signal processing for adaptive radar signature management, novel three-dimensional phased-array antenna topologies, acoustic array systems, and new research into time-modulated array antennas. He has published over 100 academic papers including several invited papers on adaptive stealth technology. His research has attracted substantial funding from both industry and government sources.